Supplementary Information for

Effects of Gamma, Electron-Beam and X-ray Radiation on EVA/EVOH/EVA Films

Yelin Ni[a], Tucker T. Bisel[a], Md Kamrul Hasan[b], Donghui Li[a], Witold K. Fuchs[a], Scott K. Cooley[a], Larry Nichols[c], Matt Pharr[b], Nathalie Dupuy[d], Sylvain Marque[e], Mark K. Murphy[a], Suresh D. Pillai[f], Samuel Dorey[g]*, Leonard S. Fifield[a]*

[a]Pacific Northwest National Laboratory, Richland, WA 99354
[b]Department of Mechanical Engineering, Texas A&M University, College Station, TX 77843
[c]Steri-Tek, Fremont, CA 94538
[d]Aix Marseille Université, Avignon Université, CNRS, IRD, IMBE, 13013 Marseille, France
[e]Aix Marseille Université, Case 551, CNRS, ICR, 13397 Marseille, France
[f]National Center for Electron Beam Research, Texas A&M University, College Station, TX 77845
[g]Sartorius Stedim FMT S.A.S., 13400 Aubagne, France

Current affiliations if different from the above:
Tucker T. Bisel is currently affiliated with Washington River Protection Solutions, Richland, WA 99352
Md Kamrul Hasan is currently affiliated with Pacific Northwest National Laboratory, Richland, WA 99354
Witold K. Fuchs is currently affiliated with NASA Glenn Research Center, Cleveland, OH 44135

corresponding authors:
Leonard S. Fifield
Pacific Northwest National Laboratory, 902 Battelle Boulevard, Richland, WA.
+1 509-375-6424
leo.fifield@pnnl.gov
Samuel Dorey
Sartorius Stedim FMT S.A.S, Z.I., Les Paluds, 13400 Aubagne Cedex, France.
+33 6 37 18 11 43
samuel.dorey@sartorius.com

This document includes three parts in the following order:

Supplementary Information Text
References
Figures S1 to S12

Other supplementary materials for this manuscript include the following:

Datasets S1 to S7

Supplementary Information Text

Thermal properties of multilayer films after irradiation. Thermal properties of ethylene vinyl acetate (EVA) and ethylene vinyl alcohol (EVOH) components in the multilayer films were studied by temperature scans on DSC and DMA. The DSC heat flow signals in the second heating cycle are displayed in Fig. S1. The main endothermic peak associated to melting of EVA shifted to lower temperatures with the increase of irradiation dose. Loss moduli (E") and tanδ curves obtained from DMA, as shown in Fig. S2, did not show such a shift. Samples cut in the machine direction (MD) and transverse direction (TD) were separately tested on DMA, but no significant difference in E', E" or tanδ signals were observed between MD and TD samples of the same irradiation condition. The β transition temperature (T_β), which could be considered as the apparent glass transition temperature (T_g), and the γ transition temperature (T_γ) were determined from DSC as the mid-point of step in baseline and from DMA tanδ peaks. As shown in Fig. S3 and Fig. S4, neither T_β nor T_γ showed notable dependencies on irradiation dose or source technology, indicating that flexibility of chain segments was not affected by the investigated irradiation conditions. Degrees of crystallinity (χ_c) for EVA and EVOH components were calculated from DSC melting peaks as described in Materials and Methods section in the main manuscript. Again, no dose or technology dependencies were detected as shown in Fig. S5.

Mechanical properties of multilayer films after irradiation. Mechanical properties were calculated from stress-strain curves of uniaxial tensile tests of the multilayer films pre-cut in the sample machine direction (MD) and transverse direction (TD). No delamination between layers was observed after tensile tests. Elongation at break (EAB), ultimate tensile strength (UTS), secant modulus (Es), and tensile toughness (U_T) are shown in Fig. S6 – Fig. S9. Elongation at break (EAB) showed a decreasing trend with the increase of irradiation dose, as seen in Fig. S6. Comparing to the unirradiated samples, the average EAB values decreased by 7% for MD samples and by 12% for TD samples at 60 kGy. Considering that a 25% loss of EAB is a criterion for material compatibility with radiation sterilization specified in AAMI TIR 17, the multilayer films were compatible with the three studied technologies up to 60 kGy, and there was still room for sterilization at higher doses if needed. MD and TD specimens both exhibited a ~20% increase in the average values of ultimate tensile strength (UTS) after 30 kGy irradiation, as shown in Fig. S7. However, further increasing the dosage from 30 kGy to 60 kGy did not result in a proportional increase in UTS regardless of the source technology. Secant modulus at 100% engineering strain ($Es_{100\%}$) was used to quantify softening behavior since a yield point or offset yield could not be found from the stress-strain curve. As shown in Fig. S8, $Es_{100\%}$ increased after 30 kGy irradiation by ~10% for MD specimens and by ~5% for TD specimens. Combined effects of irradiation on UTS and EAB were measured as tensile toughness (U_T) which was plotted in Fig. S9. Compared to unirradiated samples, toughness showed no dose dependence. Regardless of the dose dependencies, the four tensile properties discussed did not show significant differences induced by radiation technologies.

Color of multilayer films after irradiation. Yellowing and discoloration are common indicators of oxidation during sterilization. Yellowness index (YI) and total color difference (ΔE^*_{ab}) were calculated based on transmittance measured on a UV-Vis spectrometer in the visible wavelength range (380-780nm) and plotted in Fig. S10. No changes in YI or ΔE^*_{ab} were observed between source technologies or with increase of dose.

Carbonyl index of multilayer films after irradiation. Carbonyl index (CI) is a common measure of oxidation. For the films irradiated up to 60 kGy, CI did not show significant changes with dose or radiation technology as shown in Fig. S11.

Surface free energy of multilayer films after irradiation. To quantify surface wettability, surface free energy (SFE) was determined based on measured contact angles of distilled water and diiodomethane droplets on both sides of the sample films. As shown in Fig. S12, there was no significant difference between the two sides. Likewise, no dose dependency was observed. The reason why SFE of samples irradiated at 45 kGy by X-ray appeared lower than all other samples was not clear.

Statistical analysis. Effects of sterilization sources on material properties were compared between e-beam and gamma irradiation at 30 kGy, 45 kGy, and 60 kGy. Comparisons were also made between X-ray and gamma irradiation up to the same dose levels. Two one-sided t-test (TOST), also known as equivalence test, was performed where the margin of equivalence for each material property was given as 'industrial criteria' in Table 1 of the main paper. The TOST involves two separate one-sided t-tests and examines two complementary null hypotheses. For each dataset, two p-values examining the null hypotheses were calculated using '2-sample equivalence test' function in Minitab® 19.2 (© 2019 Minitab, LLC). The null hypothesis was rejected when the p-value was smaller than 0.05. The p-values, corresponding null hypotheses, and 95% confidence levels are given in attached file S7.

However, the margin of equivalence was only available for 5 out of 12 investigated material properties. A conventional t-test was performed for all material properties using two software packages: (1) the '2-sample t' function in Minitab, and (2) R software (R Core Team, 2019) including agricolae, goftest, PMCMRplus, multcomp, PMCMRplus, and car packages. P-values given by Minitab and R packages were similar. The only difference is that the degree of freedom (DF) in R packages was allowed to be a non-integer as directly calculated from the Welch–Satterthwaite equation, while in Minitab, the DF was rounded down to an integer. P-values of t-tests calculated by R packages were given in S7 file.

When conducting TOST and conventional t-tests, the significance level was chosen to be 0.05. Datasets being compared were not assumed to have equal variances.

References

1. Lagaron, J. M., Gimenez, E., Saura, J. J. & Gavara, R. Phase morphology, crystallinity and mechanical properties of binary blends of high barrier ethylene–vinyl alcohol copolymer and amorphous polyamide and a polyamide-containing ionomer. *Polymer (Guildf).* **42**, 7381–7394 (2001).

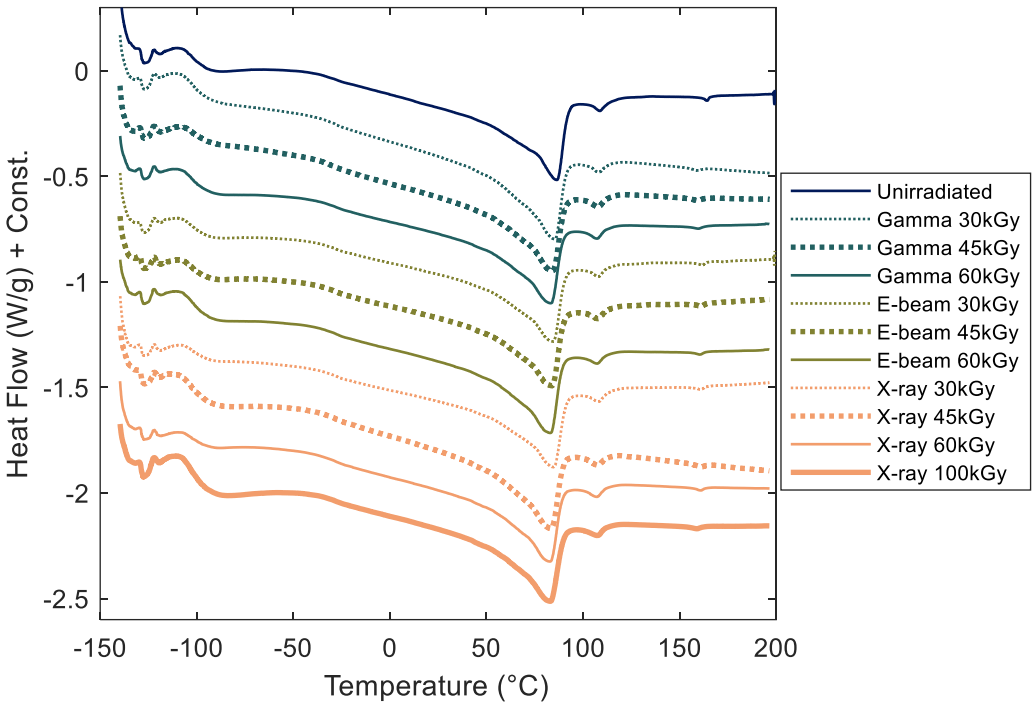

Fig. S1. Heat flow signals measured on DSC in the second heating cycle of multilayer films exposed to gamma, e-beam, and X-ray irradiation up to 100kGy. Heating and cooling rates were 10°C/min. N_2 was used as the carrier gas and purge gas. Irradiation conditions are given in the figure legend. One out of the three replicates are plotted. Curves are shifted down for clarity.

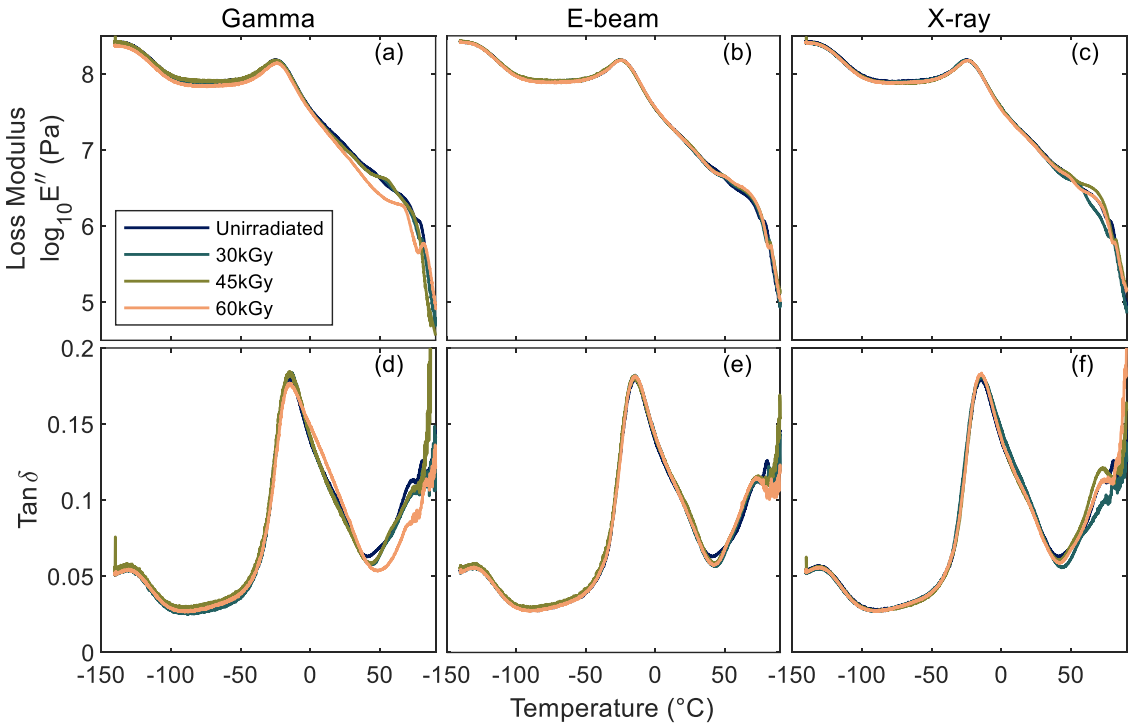

Fig. S2. Loss modulus (E”) and tangent delta (tanδ) measured on DMA during a 2°C/min temperature scan at 1 Hz and 0.1% strain for multilayer films exposed to three modalities: (a)(d) gamma, (b)(e) e-beam, and (c)(f) X-ray. One out of the three replicates are plotted.

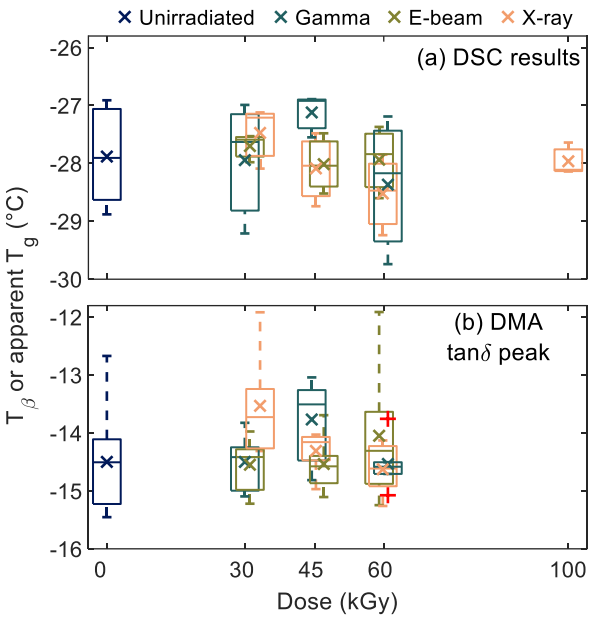

Fig. S3. The β transition temperature (T_β) or apparent glass transition temperature (T_g) of the EVA component determined from (a) DSC signals in the second heating cycle, and (b) the tanδ peak on DMA, plotted against the actual doses. As discussed in Table 2 in the main manuscript, T_β is reported as the T_g for practical reasons despite their differences in mechanisms.

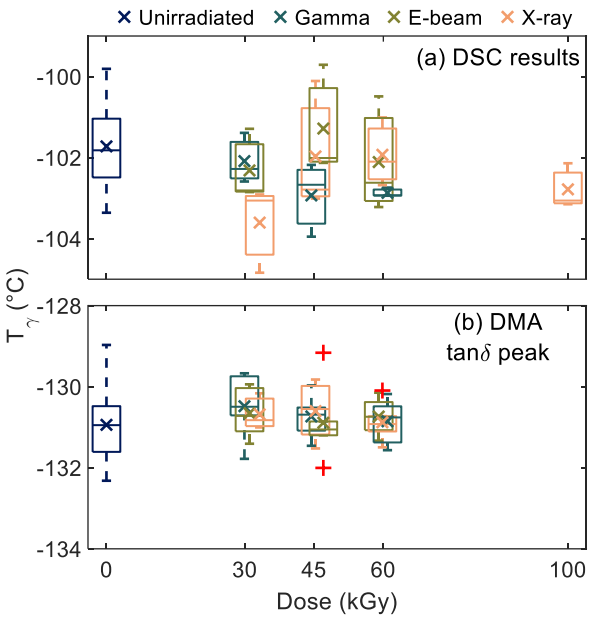

Fig. S4. The γ transition temperature (T_γ) associated with "crankshaft" relaxation of methylene groups determined from (a) DSC signals in the second heating cycle, and (b) a small tanδ peak on DMA, plotted against the actual doses.

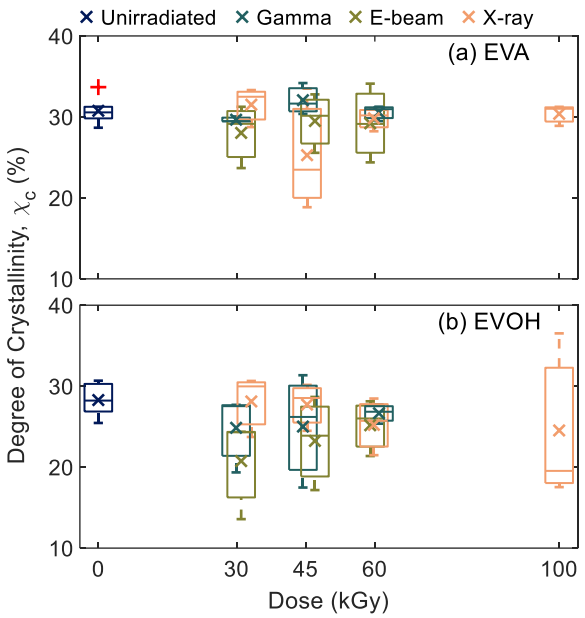

Fig. S5. Degree of crystallinity (χ_c) of (a) EVA and (b) EVOH layers calculated as the ratio of the heat of fusion (ΔH_f) of test samples to the heat of fusion of 100% crystalized PE and PVOH (ΔH_f^0), where ΔH_f^0 of PE is 290 J/g [1] and that of PVOH is 156.2 J/g [1].

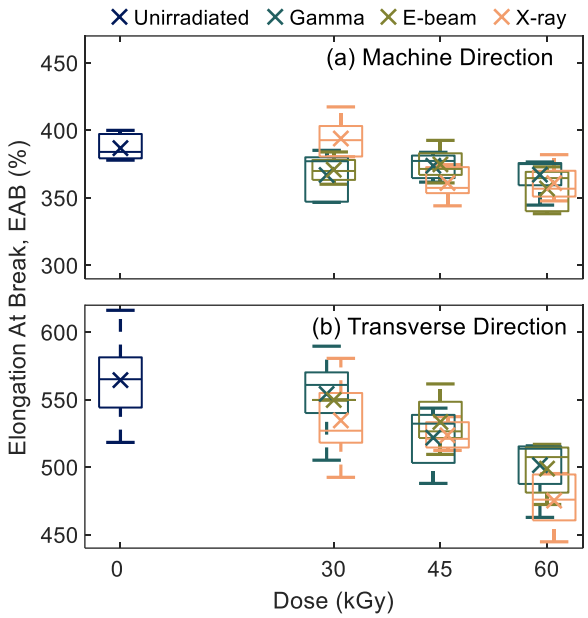

Fig. S6. Elongation at break (EAB) of multilayer films stretched along (a) the machine direction and (b) the transverse direction.

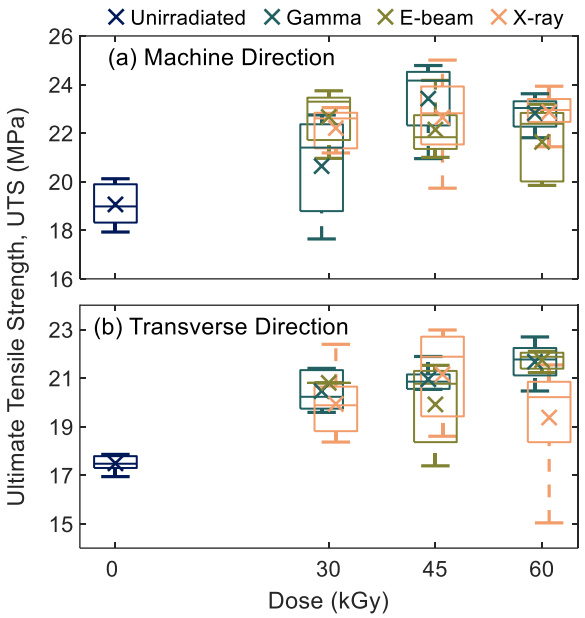

Fig. S7. Ultimate tensile strength (UTS) of multilayer films stretched along (a) the machine direction and (b) the transverse direction.

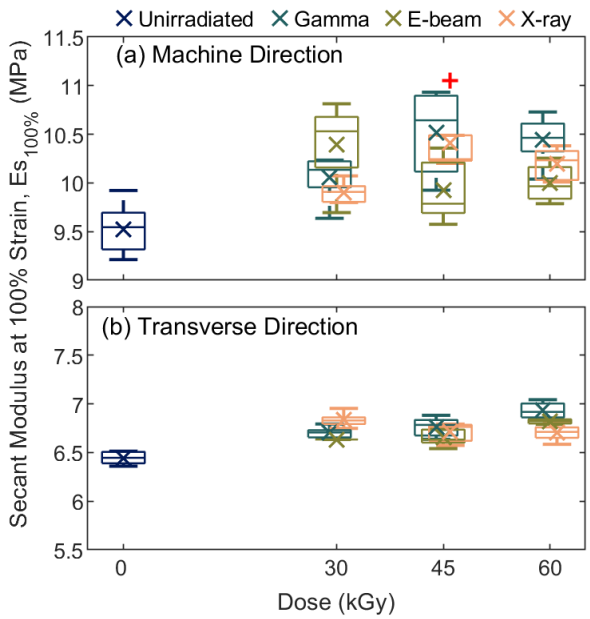

Fig. S8. Secant modulus at 100% strain ($Es_{100\%}$) of multilayer films stretched along (a) the machine direction and (b) the transverse direction.

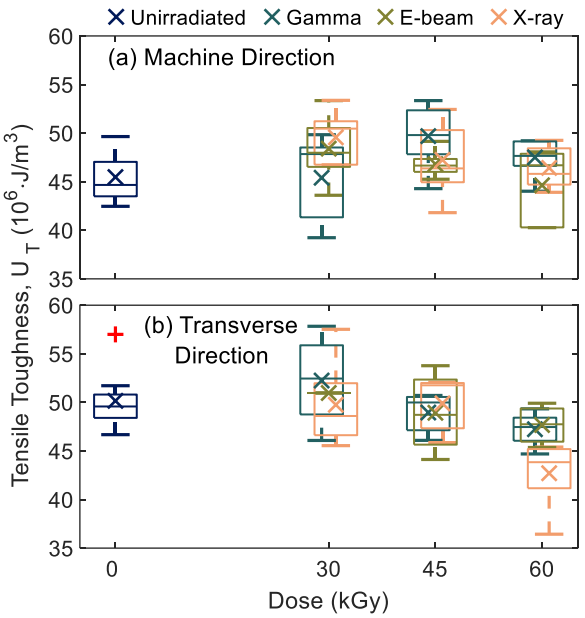

Fig. S9. Tensile toughness (U_T) of multilayer films stretched along (a) the machine direction and (b) the transverse direction.

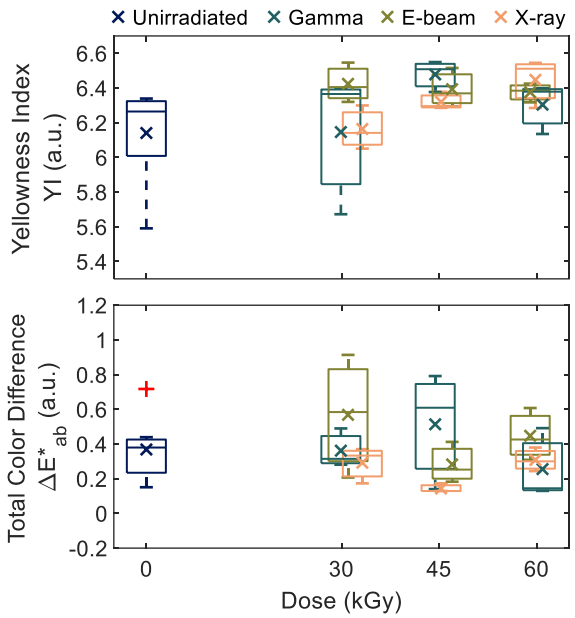

Fig. S10. Yellowness index (YI) and total color difference (ΔE^*_{ab}) of the multilayer films calculated from transmittance spectrum in the visible wavelength range (380nm – 780nm).

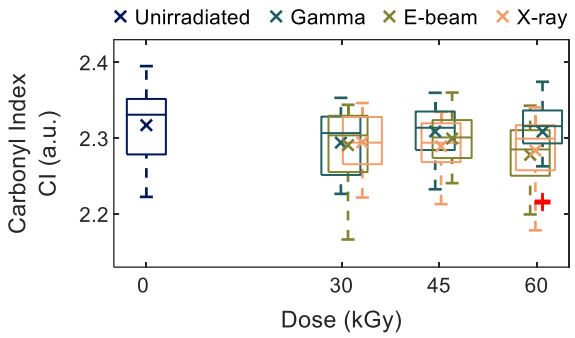

Fig. S11. Carbonyl index (CI) of multilayer films calculated as the ratio of absorbance of carbonyl groups (C=O) and hydroxyl groups (C-H) measured by FTIR.

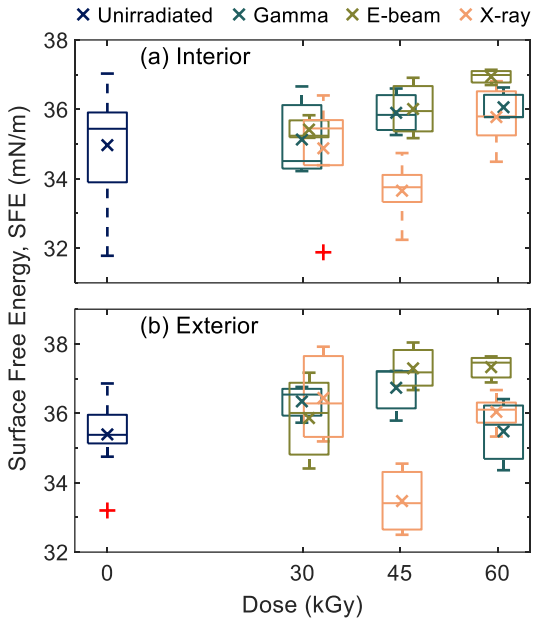

Fig. S12. Surface free energy (SFE) determined for both sides of the multilayer films used as the (a) interior and (b) exterior of single-use packaging bags made of the tested films.